Can Anthropogenic Aerosols Decrease the Snowfall Rate?

U. LOHMANN

Department of Physics and Atmospheric Science, Dalhousie University, Halifax, Nova Scotia, Canada

(Manuscript received 4 August 2003, in final form 29 April 2004)

ABSTRACT

Observations by Borys, Lowenthal, Cohn, and Brown in midlatitude orographic clouds show that for a given supercooled liquid water content, both the riming and the snowfall rates are smaller if the supercooled cloud has more cloud droplets as, for example, caused by anthropogenic aerosols. The climatic implication of this effect was studied in global climate model simulations by replacing the constant riming efficiency with a size-dependent one appropriate for planar crystals and aggregates, respectively. In the model simulations that use a size-dependent riming collection efficiency, the pollution-induced decrease in cloud droplet size causes a decrease in the riming rate in stratiform clouds despite larger liquid water contents in polluted clouds. Contrary to the above-mentioned observations, in all model simulations the snowfall rate increases because of feedbacks in the climate system. Anthropogenic aerosol particles increase the aerosol and cloud optical thickness, which reduces the solar radiation at the top of the atmosphere and the surface. This in turn causes a cooling in Northern Hemisphere midlatitudes that favors precipitation formation via the ice phase.

1. Introduction

The riming efficiency (the collection of supercooled cloud droplets by falling ice crystals or snow crystals) rapidly approaches zero for all snow crystal sizes if the cloud droplet size decreases below 10 μm in diameter (Pruppacher and Klett 1997). Mountaintop and radar measurements by Borys et al. (2003) confirm these laboratory findings. They showed from analyzing two orographic snowfall events in the Rocky Mountains in Colorado that for the same supercooled liquid water content, anthropogenically induced decreases in cloud droplet size reduced the snow water equivalent precipitation rates at the surface through the inhibition or complete shutting off of the riming process.

The riming process furthermore depends on the ice crystal shape, which in turn depends on the temperature and supersaturation conditions during its growth phase. Recent observations by Korolev et al. (2000) in stratiform clouds reveal that only a few percent of the ice crystals are pristine crystals while the majority are complex polycrystals. The differences in ice crystal shapes must be taken into account by calculating ice phase precipitation rates and ice cloud radiative properties. Various authors have shown that different assumptions of ice crystal shapes have important implications for the radiative effects of clouds, for example, Kristjánsson et al. (2000), McFarquhar et al. (2002), and Raedel et al. (2003).

Lohmann et al. (2003) introduced a size-dependent collection efficiency for the riming process assuming either planar crystals as compiled by Mitchell (1990) or aggregates as obtained from laboratory data by Lew et al. (1986) into the mesoscale model Geesthacht Simulation Model of the Atmosphere (GESIMA) in order to study the effect of anthropogenic aerosols on the riming and the snowfall rate in Arctic springtime clouds. Contrary to the findings by Borys et al. (2003), they found that the riming and the snowfall rate are initially increased in the polluted cloud due to its more numerous cloud droplets than in the clean cloud. The autoconversion rate of cloud droplets, however, decreases because of a shutdown of the collision–coalescence process in the polluted cloud. Since this process is active in the clean cloud producing drizzle-size drops, the snowfall rate is eventually enhanced due to the efficient accretion of snow crystals with the drizzle-size drops. The total amount of precipitation reaching the surface as snow at the end of the 7-h simulation depends crucially on the crystal shape. If aggregates are assumed, then a tenfold increase in aerosol concentration leads to an increase in accumulated snow by 40%, whereas the snow amount decreases by 30% when planar crystals are assumed because of the smaller riming collection efficiency in case of planar crystals.

Anthropogenic aerosol particles could also alter the snowfall rate by modifying properties of ice-forming nuclei. As discussed by Lohmann (2002a), if black carbon acts as an efficient contact nuclei, the precipitation

Corresponding author address: U. Lohmann, Dept. of Physics and Atmospheric Science, Dalhousie University, Halifax, NS B3H 315, Canada.
E-mail: Ulrike.Lohmann@dal.ca

formation rate via the ice phase will be enhanced due to anthropogenic activity. On the other hand, coating of dust aerosol particles by sulfate only slightly reduces their potential to act as a contact nuclei (Lohmann 2002b). Here, I opt to use a constant number of contact nuclei as described by Cotton et al. (1986) in order to isolate the effect of anthropogenic aerosols on the riming rate.

In this study a size-dependent riming collection efficiency in stratiform clouds of cloud droplets by both planar crystals and aggregates is applied in the ECHAM4 general circulation model (GCM) to study its effect on the present-day climate, as well as the effect of anthropogenic aerosols on the riming and the snowfall rate globally. The questions to be addressed are as follows.

- How important is the reduction of riming due to anthropogenic aerosols on a global scale?
- Are there feedbacks operating in the climate system that offset the reduction of riming due to anthropogenic aerosols?
- Does a size-dependent riming collection efficiency improve the simulations of the present-day climate?

To address these issues, first the climate model is described in the next section. It is followed by results discussing the model's sensitivity to different riming collection efficiencies in the present-day climate. This sets the stage for analyzing the climatic implications of changes in the riming rate caused by anthropogenic aerosols. The paper concludes with a discussion and summary.

2. Model description

The ECHAM4 GCM (Roeckner et al. 1996) used in this study is described in Lohmann and Lesins (2002). Prognostic aerosol variables are the mass mixing ratios of sulfate (SO_4), methane sulfonic acid (MSA), hydrophilic and hydrophobic organic carbon (OC), hydrophilic and hydrophobic black carbon (BC), sub- and supermicron dust, and sub- and supermicron sea salt. Transport, dry and wet deposition, and chemical transformations of the aerosols and gaseous precursors are calculated online with the GCM (Feichter et al. 1996). The mass of each aerosol component is converted into an aerosol particle number assuming a separate lognormal distribution with a fixed dry density, dry modal radius, and geometric width for each type (Hess et al. 1998).

The prognostic cloud variables are the mass mixing ratios of cloud liquid water and cloud ice and the number concentrations of cloud droplets and ice crystals described in Lohmann (2002b). Fractional cloud cover is only a function of relative humidity following Sundqvist et al. (1989). Parameterized microphysical processes of stratiform clouds are condensational growth of cloud droplets; depositional growth of ice crystals; homogeneous, heterogeneous, and contact freezing of cloud droplets; autoconversion of cloud droplets; aggregation of ice crystals; accretion of cloud ice by snow; riming; accretion of cloud droplets by rain; evaporation of cloud liquid water and rain; sublimation of cloud ice and snow; and melting of cloud ice and snow and sedimentation of ice crystals, snow crystals, and rain drops. The increase in the relative dispersion of the cloud droplet size distribution with increasing cloud droplet number as described in Peng and Lohmann (2003) is included in these simulations.

The parameterizations of a variety of accretional growth mechanisms are based on the approach described by Lin et al. (1983). In the model, riming (the snow crystals settling through a population of supercooled cloud droplets, freezing them upon collision) is based on the geometric sweep-out integrated over all snow sizes with an assumed exponential snow size distribution:

$$\left(\frac{\partial q_l}{\partial t}\right)_{\text{riming}} = -\frac{\pi E_{\text{SW}} n_{0S} a q_l \Gamma(3+b)}{4\lambda_S^{(3+b)}}\left(\frac{\rho_0}{\rho}\right)^{0.5}, \quad (1)$$

where q_l is the liquid water content in kilograms per kilogram, $n_{0S} = 3 \times 10^6\ \text{m}^{-4}$ is the intercept parameter, λ_S is the slope of the exponential Marshall–Palmer snow crystal size distribution, $a = 4.84$, $b = 0.25$, ρ is the air density, and $\rho_0 = 1.3\ \text{kg m}^{-3}$ is the reference density. The collection efficiency E_{SW} is highly dependent on the cloud droplet and snow crystal size (Pruppacher and Klett 1997). Here we introduce the size-dependent collection efficiency for planar ice crystals as suggested by Mitchell (1990) (simulation ESWpl) and for aggregates as obtained from laboratory results by Lew et al. (1986) (simulation ESWagg) instead of the constant value of 0.1 that is used in the ECHAM4 control simulation (CTL).

The collection efficiency for planar crystals $E_{\text{SW}}^{\text{pl}}$ and for aggregates $E_{\text{SW}}^{\text{agg}}$ is given by

$$E_{\text{SW}}^{\text{pl}} = \begin{cases} \sqrt{1 - 0.2[\log(\text{St}) - \log(\text{St}_{\text{crit}}) - 2.236]^2} & \text{Re} < 40 \\ 1.034\text{St}^{1.085} & \text{St} \le 0.06 \text{ and Re} \ge 40 \\ 0.787\text{St}^{0.988} & 0.06 < \text{St} \le 0.25 \text{ and Re} \ge 40 \\ 0.7475 \log(\text{St}) + 0.65 & 0.25 < \text{St} \le 1 \text{ and Re} \ge 40 \\ (\text{St} + 1.1)^2/(\text{St} + 1.6)^2 & \text{St} > 1 \text{ and Re} \ge 40, \end{cases} \quad (2)$$

$$E_{\text{SW}}^{\text{agg}} = 0.939\text{St}^{2.657}. \quad (3)$$

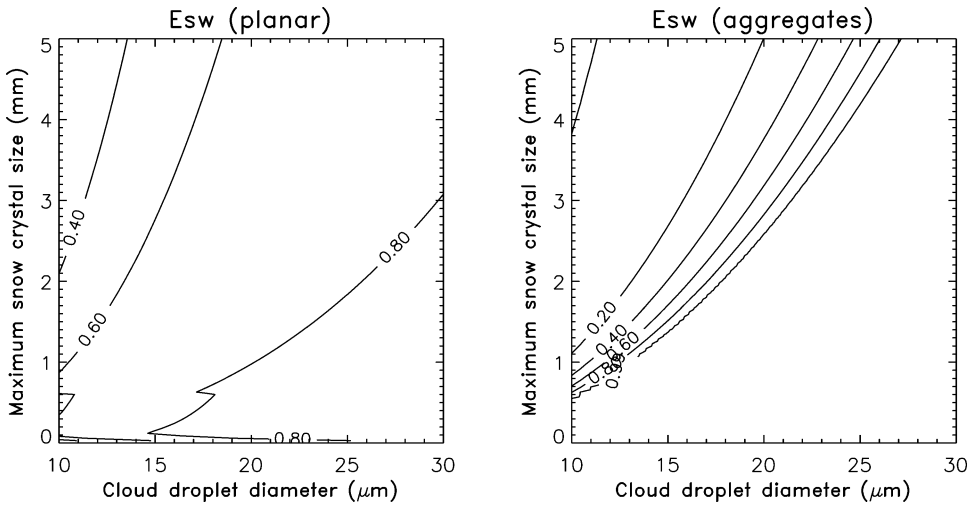

FIG. 1. Riming collection efficiency E_{SW} as a function of the cloud droplet diameter and maximum snow crystal dimension for planar crystals and aggregates. Isolines are 0.01, 0.2, 0.4, 0.6, 0.8, 0.99.

Here Re is the Reynolds number [$\mathrm{Re} = (V_t D)/\nu$], where V_t is the snow crystal terminal velocity, ν is the kinematic viscosity, and D is the maximum dimension of the snow crystal. The Stokes number (St) is given by

$$\mathrm{St} = \frac{2(V_t - v_t)v_t}{Dg}; \tag{4}$$

v_t is the cloud droplet terminal velocity; g is the acceleration due to gravity. The critical Stokes number ($\mathrm{St}_{\mathrm{crit}}$) is given by

$$\mathrm{St}_{\mathrm{crit}} = \begin{cases} 5.52\mathrm{Re}^{-1.12}, & \mathrm{Re} \le 5 \\ 1.53\mathrm{Re}^{-0.325}, & \mathrm{Re} > 5. \end{cases} \tag{5}$$

The maximum dimensions of a planar crystal D_{pl} (m) and an aggregate D_{agg} (m) are obtained from empirical mass–maximum dimension relationships and the snow crystal number concentration N_S (m^{-3}) as described in Rogers and Yau (1989) and Pruppacher and Klett (1997), respectively:

$$D_{\mathrm{pl}} = 10^{-2}\sqrt{\frac{q_S \times 10^3 \rho}{3.8 \times 10^{-4} N_S}}, \tag{6}$$

$$D_{\mathrm{agg}} = 10^{-3}\left(\frac{q_S \times 10^6 \rho}{0.04 N_S}\right)^{0.714}, \tag{7}$$

where q_s is the snow mixing ratio in kilograms per kilogram. The terminal velocity for planar crystals is given by the empirical formulas from Rogers and Yau (1989) $V_t = 2.34\,(100\,D_{\mathrm{pl}})^{0.3}$, where V_t is in meters per second. Aggregates are approximated by equivalent spheres as assumed in the control simulation. The expression for aggregates was only derived for a limited range of Stokes numbers between 0.06 and 0.3 but is extended over the full range of collection efficiencies, bounded between a lower and upper limit of E_{SW} of 0.01 and 1, respectively.

The riming collection efficiencies [Eqs. (2) and (3)] are shown in Fig. 1. Note that E_{SW} increases with cloud droplet diameter but decreases with snow crystal size. As the snow crystal size increases, the Stokes number and thus E_{SW} decrease because the snow crystal terminal velocity depends sublinearly on the maximum snow crystal size. In the case of planar crystals, E_{SW} is between 0.4 and 0.8 for a large range of crystal and droplet sizes, whereas E_{SW} for aggregates approaches 0 for cloud droplets below 11 μm in diameter and the snow crystal maximum dimension exceeding 4 mm. On the other hand, E_{SW} approaches 1 when the size difference between snow crystals and cloud droplets increases, thus covering a wider range in efficiencies than in the case of planar crystals.

The riming rate [Eq. (1)] is plotted as a function of the supercooled liquid water content and the cloud droplet diameter for a 0.5- and 5-mm snow crystal in Fig. 2. The riming rate increases with increasing cloud droplet diameter and liquid water content. Note that riming increases with increasing snow crystal size despite the decrease in collection efficiency for the larger snow crystal size. In the case of aggregates, riming becomes almost independent of the liquid water content (LWC) for LWC > 0.05 g m^{-3} in the case of a 0.5-mm aggregate, and for LWC > 0.15 g m^{-3} in the case of a 5-mm aggregate. This effect is less pronounced in case of planar crystals, but also here the dependence of the riming rate on cloud droplet size is stronger than on the liquid water content.

3. Implications of different riming rates for the present-day climate

All results are based on 10-yr experiments in T30 horizontal resolution and 19 vertical levels after an initial spinup of 3 months using prescribed climatological

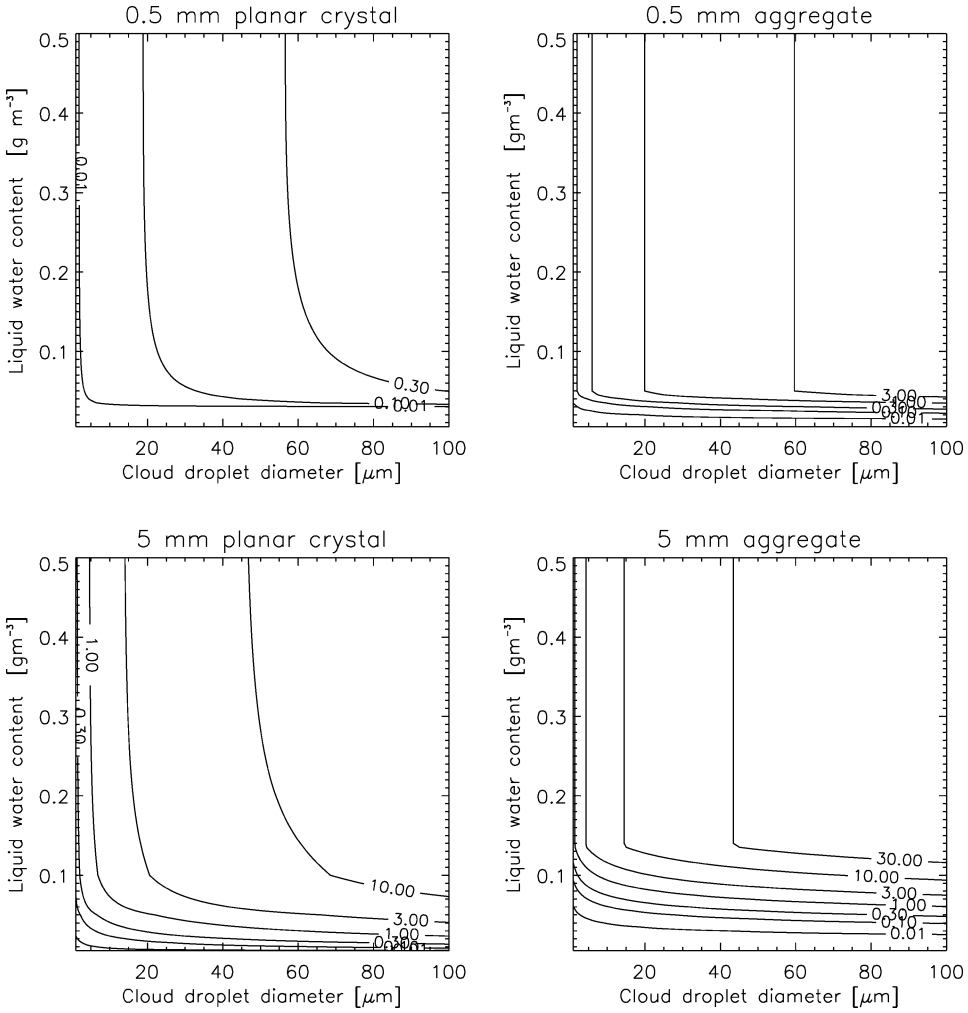

FIG. 2. Riming rates (μg kg^{-1} s^{-1}) for a (top) 0.5- and (bottom) 5-mm snow crystal at an air density of 1 kg m^{-3} as a function of the supercooled liquid water content and the cloud droplet diameter. Isolines are 0.01, 0.1, 0.3, 1, 3, 10, 30 μg kg^{-1} s^{-1}.

sea surface temperatures and sea ice extent. The zonal mean distribution of E_{SW} in the simulations ESWpl and ESWagg is shown as a function of height and latitude in Fig. 3. The riming collection efficiency in both ESWpl and ESWagg is higher than in the control simulation ($E_{SW} = 0.1$) in most parts of the troposphere. As a consequence, the liquid water content and cloud droplet number concentration are reduced almost everywhere in both ESWpl and ESWagg as compared to CTL (Fig. 4).

The change in riming collection efficiency affects the liquid water path most noticeably. In the global mean, it decreases from 78 in CTL to 56 g m^{-2} in ESWpl and to 52 g m^{-2} in ESWagg. Observations of liquid water path over oceans from a Special Sensor Microwave Imager (SSM/I) by Wentz (1997), Greenwald et al. (1993), and Weng and Grody (1994) together with the different model simulations are shown in Fig. 5. The spread between the different simulations is comparable to the spread in the different SSM/I-retrieved liquid water paths. While the simulation CTL exceeds all retrievals in midlatitudes, the simulations ESWpl and ESWagg predict smaller liquid water paths, closer to the Weng and Grody (1994) retrieval.

The above described cloud microphysics, including the change in collection efficiency, are only included for large-scale stratiform clouds, so that changes in snowfall rates are dominated by changes in stratiform clouds. As can be seen in Fig. 6, the vertically integrated riming rate is increased in ESWagg and ESWpl as compared to CTL. This increases the snowfall rate in ESWpl and ESWagg despite the reduction in liquid water path by up to 0.2 mm day^{-1} in mid- and high latitudes of the Northern Hemisphere and by about 0.5 mm day^{-1} at 60°S as compared to CTL. The decrease in snowfall rate in ESWpl and ESWagg close to the Poles likely

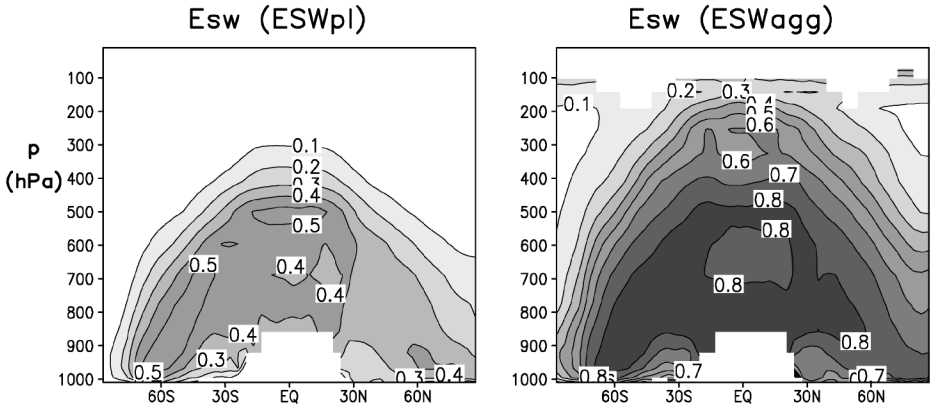

FIG. 3. Riming collection efficiency E_{sw} as a function of altitude and latitude for the simulations ESWpl and ESWagg.

results from feedbacks of cloud microphysical changes on temperature and large-scale dynamics in these different simulations.

In the global mean, the total amount of precipitation increases from 2.74 mm day^{-1} in CTL to 2.94 mm day^{-1} in ESWpl and to 3.0 mm day^{-1} in ESWagg due to the larger riming collection efficiency. Here the lowest amount of precipitation in the simulation CTL agrees best with the observations of the Global Precipitation Climatology Center dataset of 2.78 mm day^{-1} in the global mean averaged over 1986 to 1994 (Stendel and Arpe 1997), while ESWpl and ESWagg simulate excessive precipitation in the Tropics (Fig. 5).

The faster hydrological cycles in ESWpl and ESWagg with a decrease in cloud liquid water and an increase in precipitation result in a decrease in relative humidity in the atmosphere, which in turn decreases the fractional cloud cover. As shown in Fig. 5, the decrease in cloud cover in ESWpl and ESWagg occurs everywhere but is most pronounced in the Tropics where the changes in relative humidity are highest and where cloud cover is already underestimated in CTL. In the global mean,

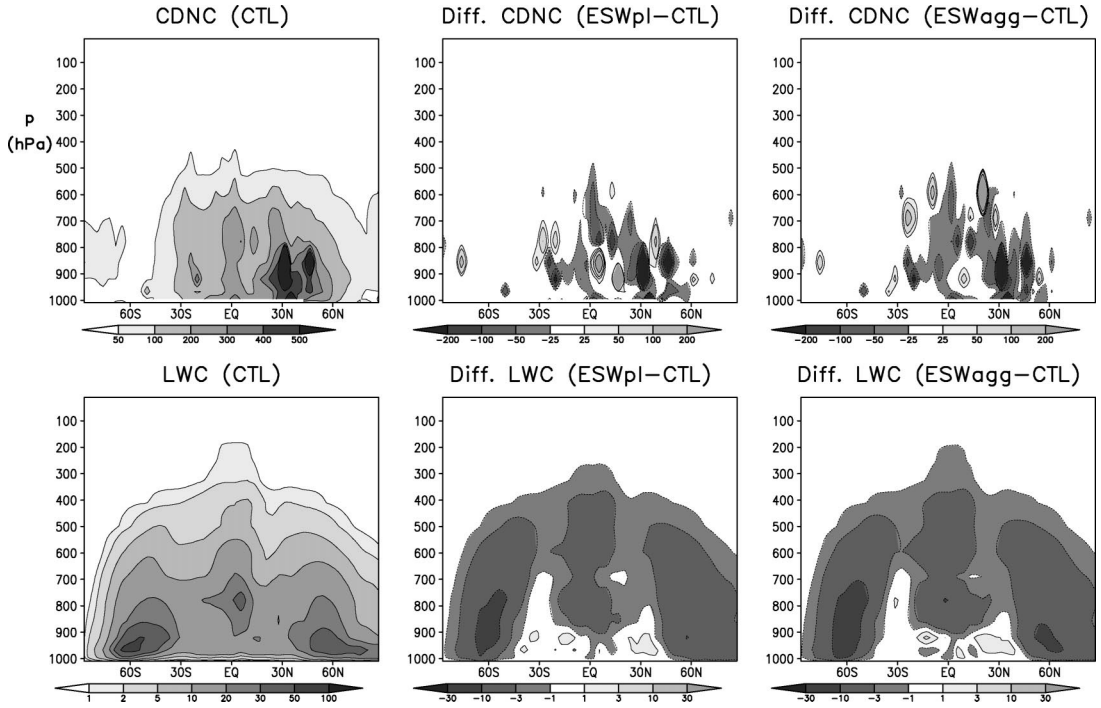

FIG. 4. Zonal, annual mean latitude vs pressure distribution of the cloud droplet number concentration (CDNC; cm^{-3}) and liquid water content (LWC; mg kg^{-1}) for the simulation CTL and the differences ESWpl − CTL and ESWagg − CTL.

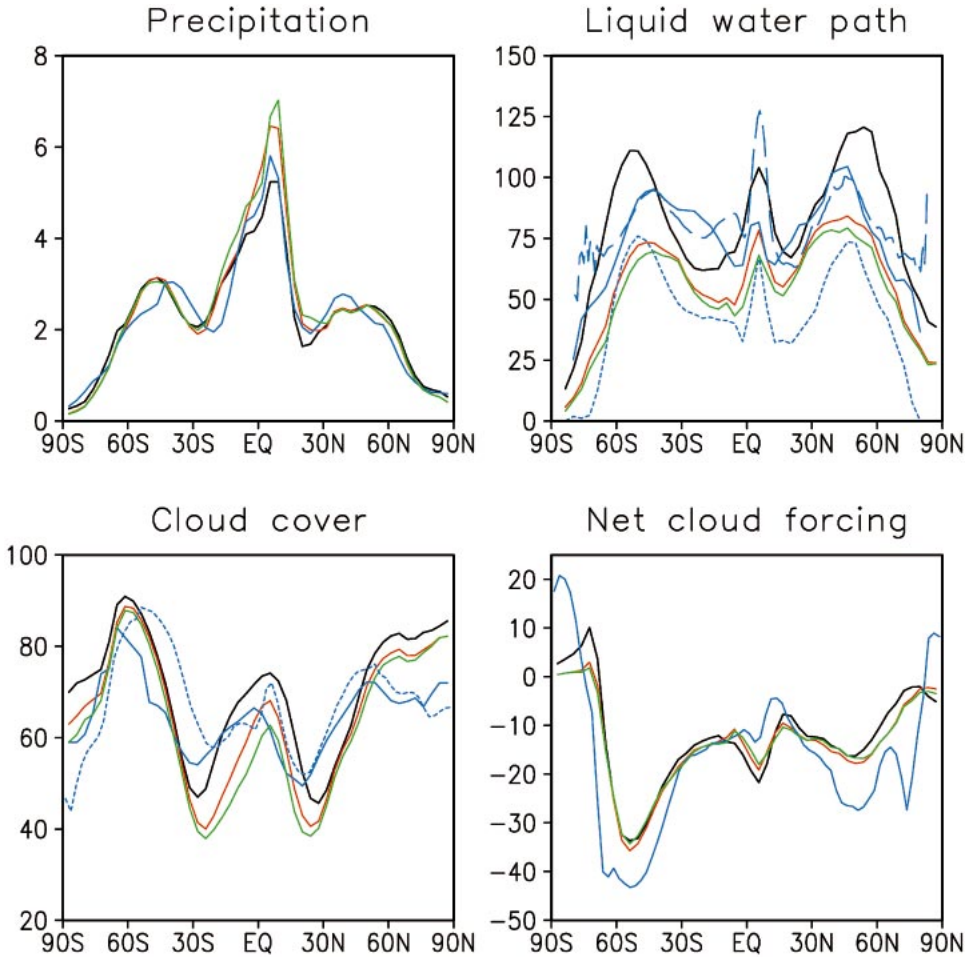

FIG. 5. Zonal, annual means of precipitation (mm day^{-1}), liquid water path (g m^{-2}), cloud cover (%), and net cloud forcing (W m^{-2}) at the top of the atmosphere from the simulations CTL (black line), ESWpl (red line), and ESWagg (green line) as compared with different observations (blue line). Observations of precipitation are from the Global Precipitation Data Set (Stendel and Arpe 1997); SSM/I retrievals of LWP are from Greenwald et al. (1993; solid line), Wentz (1997; dashed line), and Weng and Grody (1994; dotted line); cloud cover is obtained from surface observations Hahn et al. (1994) (solid line) and ISCCP (Rossow and Schiffer 1999; dotted line) and cloud forcing observation are obtained from ERBE.

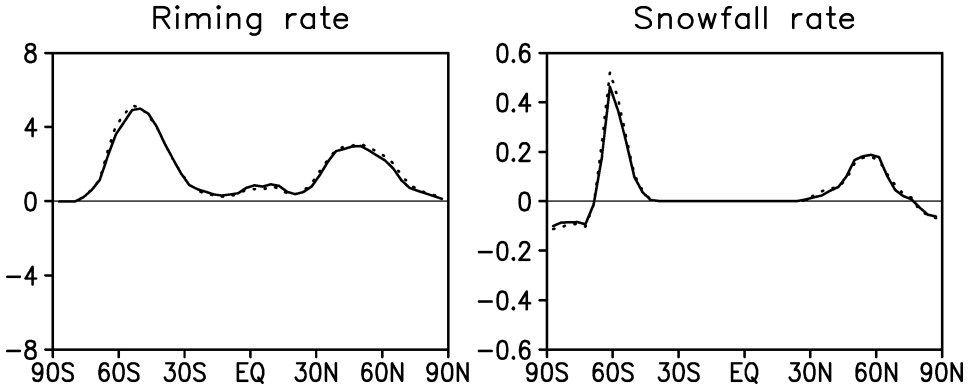

FIG. 6. Zonal, annual mean differences in vertically integrated riming rate (mg m^{-2} s^{-1}) and snowfall rate (mm day^{-1}) for the differences ESWpl − CTL (solid line) and ESWagg − CTL (dotted line).

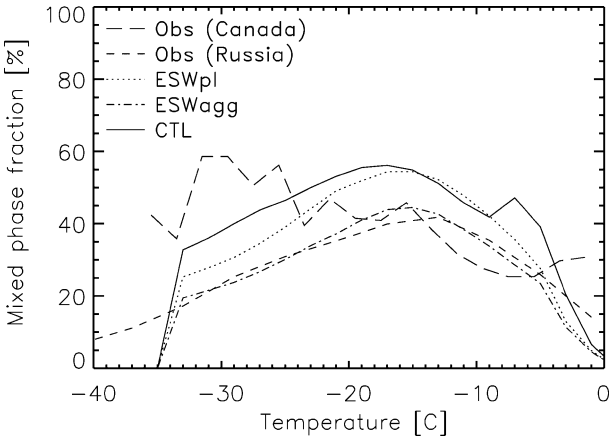

FIG. 7. Percentage of mixed-phase clouds as a function of temperature from observations over Russia (Matveev 1984), over Canada (Korolev et al. 2003), and from model data poleward of 30°N from the simulations CTL, ESWpl, and ESWagg.

cloud cover is decreased from 67% in CTL to 61% in ESWpl and further to 58% in ESWagg. The different cloud cover observations from the surface (Hahn et al. 1994) and from the International Satellite Cloud Climatology Project (ISCCP; Rossow and Schiffer 1999) estimate a global mean cloud cover of 62% and 67%, respectively. Here again, the simulation CTL agrees best with the observations.

A lower liquid water path leads to a smaller shortwave cloud forcing. At the same time, the reduced cloud cover decreases the longwave cloud forcing so that the net cloud forcing remains almost the same. In the global mean, it is -15 W m^{-2} in CTL and -16 W m^{-2} in ESWpl and ESWagg. All of these are lower than the -19 W m^{-2} estimated from the Earth Radiation Budget Experiment (ERBE; Hartmann 1993). The underestimations are worst in midlatitude storm tracks because the simulated clouds are not reflective enough (Fig. 5).

Observations of mixed-phase clouds associated with frontal systems by Korolev et al. (2003) show a larger fraction of mixed-phase clouds at colder temperatures than previously observed. For example, the long-term Russian dataset (Matveev 1984) shows a steadily decreasing fraction of mixed-phase clouds below -15°C (Fig. 7). On the contrary, the Canadian dataset shows a roughly constant mixed-phase fraction (Korolev et al. 2003). The mixed-phase fraction calculation in the Canadian dataset is based on 1-s-averaged aircraft data that avoids cloud-free zones and artificial merging of separate zones of pure ice and pure liquid into a mixed-phase cloud category (A. Korolev 2003, personal communication). Because of the lower vapor pressure over ice, mixed-phase clouds are not stable and will completely glaciate with time unless there is a constant updraft supplying the moisture source. Thus, the Canadian data suggest that most mixed-phase clouds are either newly formed or have a steady moisture supply. The overall fraction of supercooled clouds from the different model simulations in Northern Hemispheric mid- and high latitudes is comparable to the observations. While the simulation ESWagg agrees best with the Russian dataset, the higher mixed phase fraction in simulations CTL and ESWpl at colder temperatures is more consistent with the Canadian data.

In order to see whether the climate model simulations reproduce the observed negative correlation between cloud droplet concentration and snowfall rate obtained by Borys et al. (2000), the snowfall rate poleward of 30° as a function of the vertically integrated number of cloud droplets for different values of liquid water path is plotted in Fig. 8. For small cloud droplet concentrations, the snowfall rate increases with increasing cloud droplet number in all simulations. This suggests that initially more liquid water is available for riming, thus increasing the snowfall rate. For liquid water paths of more than 90 g m^{-2}, the increase in snowfall rate with increasing cloud droplet number is less pronounced in simulations ESWpl and ESWagg as compared to CTL because here the smaller cloud droplet radius at larger cloud droplet number concentrations reduces the riming rate via Eqs. (2) and (3). Once the column-integrated cloud droplet number concentration exceeds roughly 50 $\times$ 10^6 cm^{-2}, the snowfall rate decreases or remains nearly constant as observed by Borys et al. (2000). At the largest droplet numbers, the snowfall rate sometimes increases again. This is probably not statistically significant due to the larger standard deviation and the fewer number of points in these cloud droplet number bins.

4. Implications of different riming rates for the indirect aerosol effect

Anthropogenic emissions of aerosol particles and their precursors have considerably increased the global mean aerosol burden since preindustrial times. Since some aerosols act as cloud condensation nuclei, the increase in cloud droplet number for a given cloud water content increases the cloud albedo (first indirect aerosol effect). In addition, the precipitation efficiency of warm clouds is reduced, increasing cloud lifetime (second indirect aerosol effect). Both effects are very uncertain (Ramaswamy et al. 2001). They are estimated to have reduced the net radiation at the top of the atmosphere between 0 and -4 W m^{-2} (e.g. Lohmann and Lesins 2002; Anderson et al. 2003). The question here is whether aerosols have an effect on the snow formation via the riming process as suggested by the observations of Borys et al. (2003). In order to estimate this effect globally, the three 10-yr simulations CTL, ESWpl, and ESWagg were rerun, but without any anthropogenic emissions. That is, emissions of sulfate and carbonaceous (black carbon and organic carbon) aerosols from fossil fuel and biomass burning are set to zero. It leaves natural emissions from forests as the only source for organic carbon, and dimethyl sulfide emissions from the

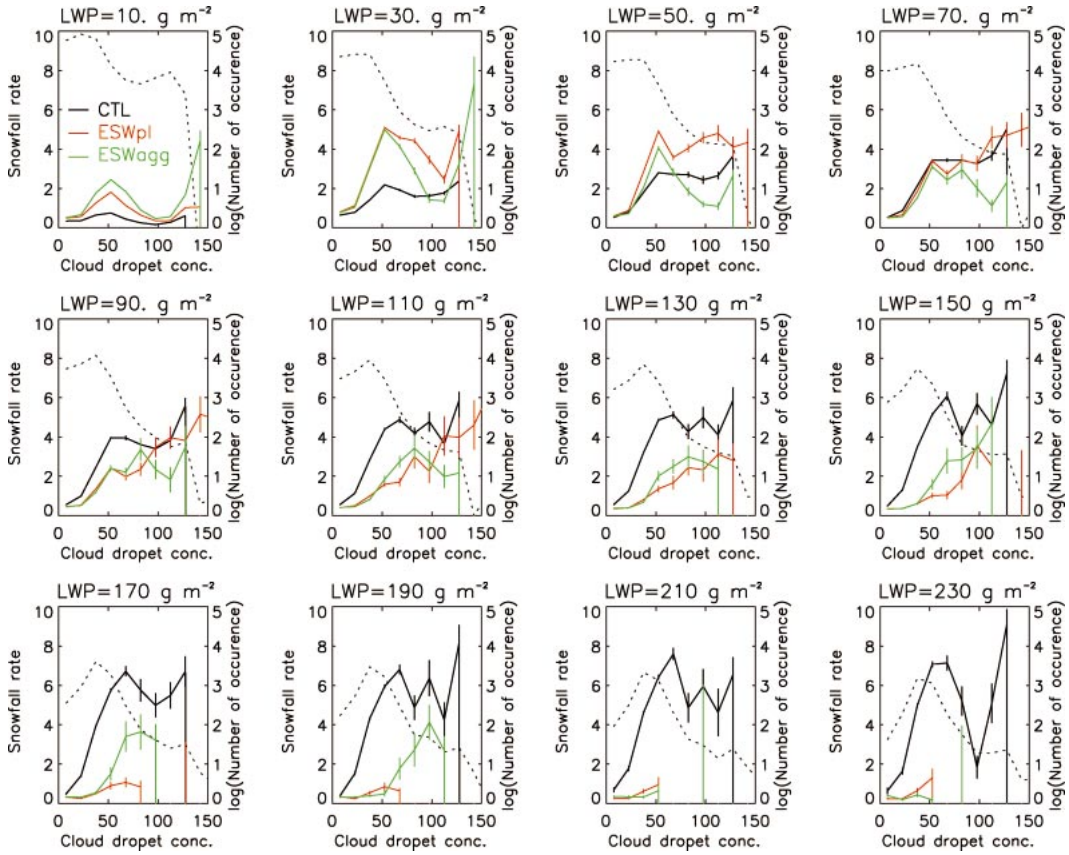

FIG. 8. Snowfall rate (mm day^{-1}) as a function of the vertically integrated cloud droplet number concentration (10^6 cm^{-2}) for different 20 g m^{-2} ranges of LWP from the simulations CTL, ESWpl, and ESWagg poleward of 30°. The value of LWP in the plot header is the midpoint of each 20 g m^{-2} increment. The vertical bars denote ±one standard deviation in snowfall rate based on 12-hourly model output data from 1 yr for that cloud droplet number concentration interval. The dotted line refers to the logarithm of the number of points in each LWP size bin in the simulation CTL.

ocean and volcanoes as the only sources for sulfate aerosols. Greenhouse gas concentrations are held constant at their present-day value.

As shown in Fig. 9, the effective cloud droplet radius, averaged over all liquid cloud layers, decreases by more than 1 μm from preindustrial to present-day times in the Northern Hemisphere. In CTL, where the riming collection efficiency is constant, the increase in liquid water path as a result of the aerosol-induced reduction in autoconversion and accretion of cloud droplets with raindrops results in a 4% larger vertically integrated global mean riming rate of 0.06 mg m^{-2} s^{-1} in the present-day climate (Table 1). In ESWagg and ESWpl the decrease in cloud droplet radius is more important for the riming rate than the increase in liquid water path (cf. also Fig. 2). In these two simulations the riming rate decreases by up to 0.5 mg m^{-2} s^{-1} in the Northern Hemisphere and globally by 0.04 to 0.09 mg m^{-2} s^{-1} (1.4%–2.7% of their preindustrial values), respectively (Table 1). The global mean snowfall rate, however, increases by 0.003 mm day^{-1} (2%) between preindustrial and present-day times in all simulations. If the snowfall rate was governed by the riming process, then the snowfall rate should only increase in the control simulation CTL but decrease in both ESWagg and ESWpl. Instead, the increase in snowfall rate is caused by the decrease in shortwave radiation at the surface in Northern Hemisphere midlatitudes due to the increase in aerosol and cloud optical depth (Fig. 9). The reduction in shortwave radiation leads to a cooling of the surface and lower atmospheric temperature over land (the ocean temperature is kept at its climatological value). Also, as shown in Fig. 10, the atmospheric temperature becomes colder over Northern Hemispheric midlatitudes, which in turn increases the ice water content by depositional growth and enhances the snow crystal growth by aggregation, resulting in a slightly higher snowfall rate in all simulations (Fig. 9).

The total amount of precipitation, on the other hand, decreases by 0.05 mm day^{-1} (2%) in the global mean in all simulations (Table 1) as a result of the aerosol-induced reduction in cloud droplet autoconversion rate and accretion rate of cloud droplets with raindrops, the aerosol lifetime or second indirect aerosol effect. Apart

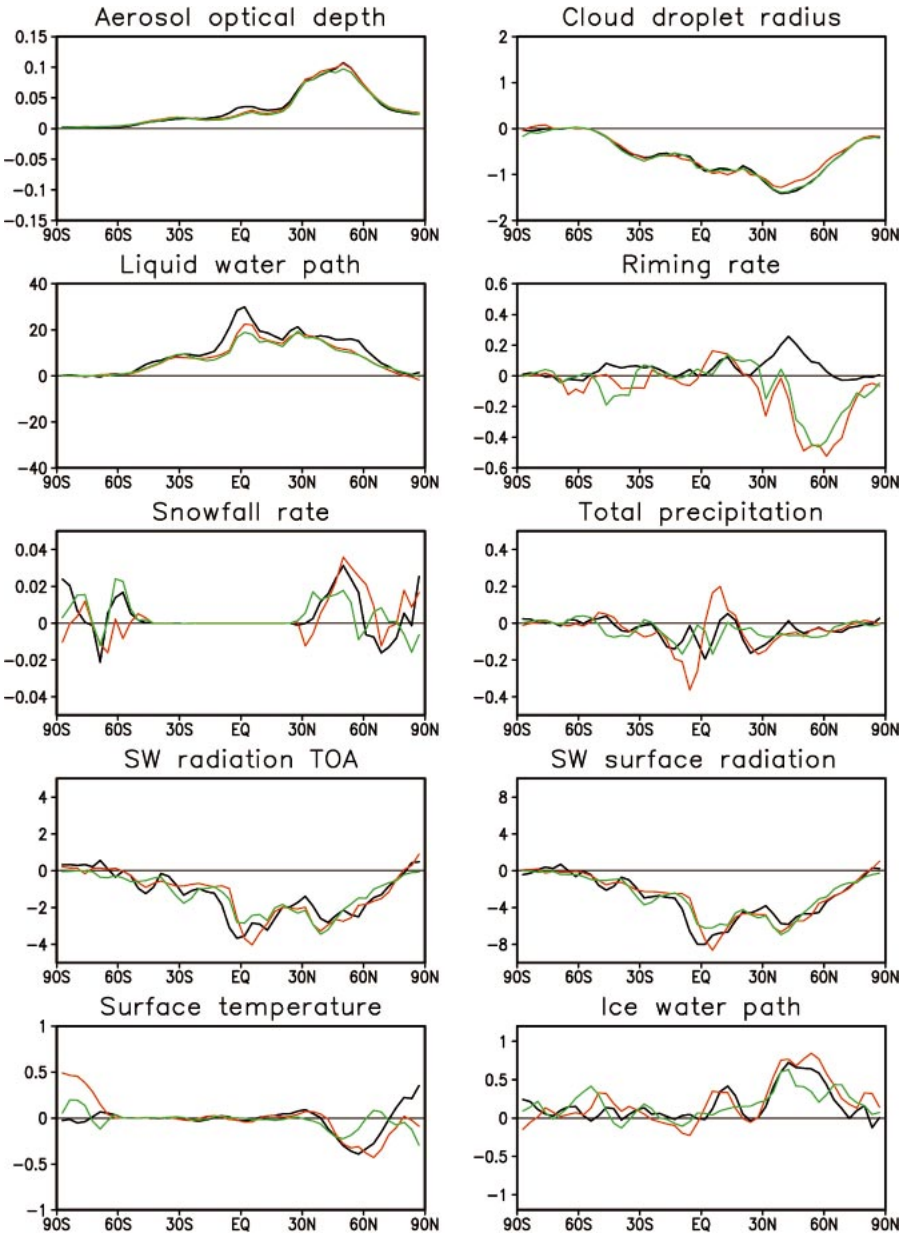

FIG. 9. Zonal, annual mean changes in aerosol optical depth, effective cloud droplet radius averaged over all liquid water cloud layers (μm), LWP (g m^{-2}), vertically integrated riming rate (mg m^{-2} s^{-1}), snowfall rate (mm day^{-1}), total precipitation (mm day^{-1}), shortwave (SW) radiation at the top of the atmosphere (TOA) and at the surface (W m^{-2}), surface temperature (K) and ice water path (g m^{-2}) between preindustrial and present-day times for the simulations CTL (black line), ESWpl (dotted line), and ESWagg (dot–dashed line).

from a northward shift of the intertropical convergence zone in ESWpl, the precipitation mainly decreases in the Northern Hemisphere in all simulations (Fig. 9).

The global mean decrease of net radiation at the top of the atmosphere, the total anthropogenic aerosol effect, amounts to -1.24 W m^{-2} in the control simulation (Table 1). This difference includes the direct, indirect, and semidirect aerosol effect. As shown by Lohmann and Feichter (2001), the net direct and the semidirect effects are rather small with a contribution of only 0.1 W m^{-2}. Thus, this difference is mainly attributable to the first and second indirect aerosol effects. The net effect of aerosols on the radiation, however, is less negative than previously estimated, because the increase in the relative dispersion of the cloud droplet size distribution with increasing aerosols and hence cloud droplet number concentration (Liu and Daum 2002; Peng and Lohmann 2003) is considered in these simulations. The

TABLE 1. Global annual mean changes ± interannual standard deviation between preindustrial and present day for the different pairs of simulations with percentage change from preindustrial values in parenthesis of effective cloud droplet radius averaged over all liquid water cloud layers (Δr_{eff}, μm); total preciptation (Δprecip, mm day^{-1}); snowfall rate (Δsnow, mm day^{-1}); vertically integrated riming rate (Δriming, mg m^{-2} s^{-1}); shortwave (SW), longwave (LW), and net radiation at the top of the atmosphere (ΔF^{TOA}, W m^{-2}); net shortwave radiation at the surface ($\Delta F^{\text{sfc}}_{\text{SW}}$W m^{-2}) and surface temperature (ΔT_{sfc}, K).

Experiment	CTL	ESWpl	ESWagg
Δr_{eff}	−0.71 ± 6.06 (9.1)	−0.70 ± 0.12 (9.2)	−0.72 ± 0.09 (9.2)
Δprecip	−0.047 ± 0.009 (1.7)	−0.051 ± 0.008 (1.7)	−0.049 ± 0.007 (1.6)
Δsnow	0.003 ± 0.003 (2.3)	0.003 ± 0.004 (1.6)	0.003 ± 0.002 (2.0)
Δriming	0.055 ± 0.022 (3.8)	−0.087 ± 0.04 (2.7)	−0.044 ± 0.024 (1.4)
$\Delta F^{\text{TOA}}_{\text{SW}}$	−1.68 ± 0.30 (0.7)	−1.63 ± 0.39 (0.6)	−1.60 ± 0.12 (0.6)
$\Delta F^{\text{TOA}}_{\text{LW}}$	−0.43 ± 0.20 (0.2)	−0.59 ± 0.34 (0.2)	−0.63 ± 0.24 (0.3)
ΔF^{TOA}	−1.24 ± 0.22 (—)	−1.04 ± 0.27 (—)	−0.97 ± 0.27 (—)
$\Delta F^{\text{sfc}}_{\text{SW}}$	−3.75 ± 0.44 (2.5)	−3.6 ± 0.57 (2.2)	−3.53 ± 0.2 (2.1)
ΔT_{sfc}	−0.028 ± 0.05 (0.2)	−0.025 ± 0.05 (0.2)	−0.023 ± 0.05 (0.2)

1.24 W m^{-2} decrease in net radiation results from a 1.68 W m^{-2} increase in reflected shortwave radiation that is partly offset by 0.43 W m^{-2} less outgoing longwave radiation (Table 1). The decrease in shortwave radiation at the top of the atmosphere and at the surface is most pronounced in the Tropics and Northern Hemisphere midlatitudes mirroring the increase in liquid water path (Fig. 9).

Adding the anthropogenic aerosol effect on the riming and snowfall rate of stratiform clouds slightly decreases the indirect aerosol effect. In these simulations, the global mean net aerosol effect at the top of the atmosphere amounts to −1.0 W m^{-2} in both ESWagg and ESWpl (Table 1). While the reflected shortwave radiation due to anthropogenic aerosols is similar in all simulations, slightly more outgoing longwave radiation is trapped in ESWagg and ESWpl (0.6 W m^{-2}). These estimates of the calculated indirect aerosol effect from first principles are consistent with inverse estimates of the indirect aerosol effect as summarized by Anderson et al. (2003).

5. Discussion and summary

In this paper the global impact of aerosols on the riming rate of snow crystals of different shapes with cloud droplets in stratiform clouds was investigated using the ECHAM4 general circulation model. The constant riming collection efficiency was replaced by two different size-dependent accretion rates, one derived for planar crystals (Mitchell 1990) in simulation ESWpl and one for aggregates (Lew et al. 1986) in simulation ESWagg. In both cases, the size-dependent riming collection efficiency is larger than the constant value of 0.1 that is used in the reference simulation CTL. Thus, the liquid water path and cloud cover are decreased in ESWpl and ESWagg as compared to CTL and the precipitation is

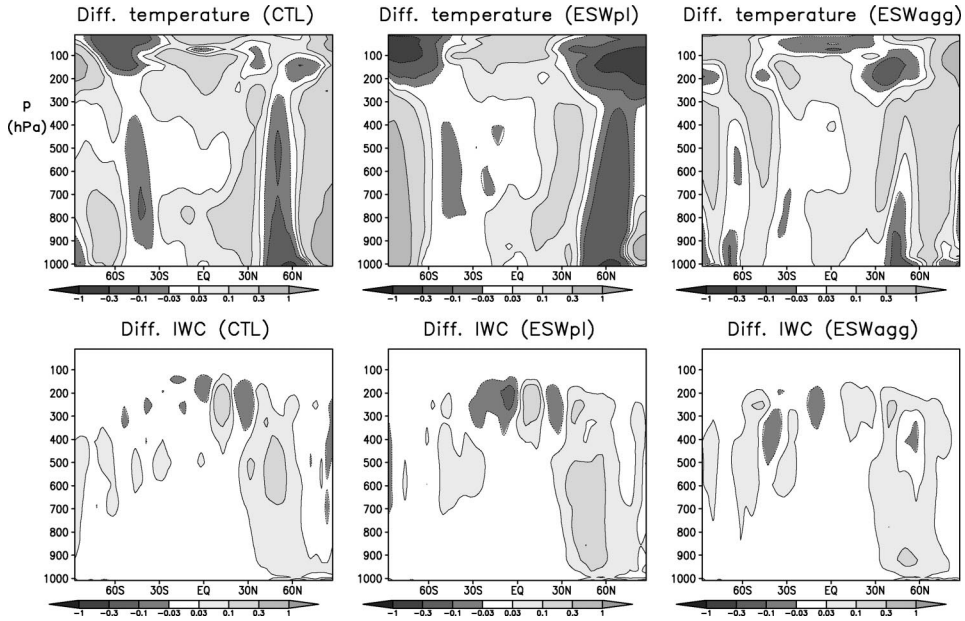

FIG. 10. Change in temperature (K) and IWC (mg kg^{-1}) as a function of altitude and latitude between preindustrial and present-day times for the simulations CTL, ESWpl, and ESWagg.

enhanced. Because the riming collection efficiency was used as a tuning parameter in CTL to bring the climate model in radiative equilibrium and in reasonable agreement with radiation observations from the Earth Radiation Budget Experiment, simulation CTL performs best overall when compared to different observations.

However, the focus of this study was not to retune the model, but rather to investigate whether an increase in cloud droplet number concentration due to anthropogenic aerosols together with a decrease in cloud droplet radius would reduce the riming efficiency and snowfall rate globally. If this was the case, this would be a third indirect aerosol effect, because the reduction in snowfall rate due to anthropogenic aerosols would increase the lifetime of these cold clouds and thereby affect the earth radiation budget.

The climate model simulations performed in this study confirm the decrease in riming rate by anthropogenic-aerosol-induced decreases in cloud droplet size if a size-dependent collection efficiency is introduced in the riming rate. This decrease in riming rate is, however, not translated in a reduced snowfall rate because the decrease in cloud droplet size, first of all, reduces the amount of solar radiation reaching the surface and thus cools the surface temperature over land and the atmospheric temperature in Northern Hemisphere midlatitudes. This in turn favors depositional and aggregational growth of ice and snow crystals thereby slightly increasing the snowfall rate in all present-day simulations over preindustrial times.

The question remains as to whether this is realistic? One could argue that Borys et al. (2003) observed a special case in which the cloud liquid water content remained constant. Since there are no observations of liquid water path in preindustrial times, it is hard to know how cloud properties changed. Houghton et al. (2001) stated that it is likely that cloud amount over land increased by 2% during the twentieth century. On the other hand, the analysis of satellite data by Nakajima et al. (2001) suggests that the liquid water path over oceans does not change with column aerosol number, which was reproduced by Lohmann and Lesins (2002) using the same model configuration as used in this study for simulation CTL. Thus, the nearly constant liquid water path with increasing aerosol index is not in contradiction with an increase in liquid water path since preindustrial times. To answer the above question, it appears that the observed case study by Borys et al. (2003) is a local case that cannot be extrapolated to a global scale and does not hold when feedbacks of cloud microphysics on the heat and moisture budget are considered. Globally, anthropogenic aerosols in the climate model ECHAM4 do not reduce the snowfall rate, but rather slightly enhance.

In this study riming is only considered in stratiform clouds, not in convective clouds. This is sufficient to test the importance of a reduction in riming in stratiform clouds as observed by Borys et al. (2003) on a global scale. However, riming rates are higher in deep convection. In these clouds, the effect of anthropogenic aerosols on riming is potentially larger as, for instance, suggested by Khain et al. (2001). To investigate this effect is beyond the scope of this paper, but will be considered in the future.

Acknowledgments. U. Lohmann thanks Glen Lesins, Yangang Liu, and two anonymous reviewers for helpful comments and suggestions. The work was supported by the National Science and Engineering Research Council of Canada (NSERC) and the Canadian Foundation for Climate and Atmospheric Science (CFCAS). She thanks the Deutsches Klimarechenzentrum for computing time.

REFERENCES

Anderson, T. L., R. J. Charlson, S. E. Schwartz, R. Knutti, O. Boucher, H. Rodhe, and J. Heintzenberg, 2003: Climate forcing by aerosols—A hazy picture. *Science,* **300,** 1103–1104.

Borys, R. D., D. H. Lowenthal, and D. L. Mitchell, 2000: The relationships among cloud microphysics, chemistry, and precipitation rate in cold mountain cloud. *Atmos. Environ.,* **34,** 2593–2602.

——, ——, S. A. Cohn, and W. O. J. Brown, 2003: Mountaintop and radar measurements of anthropogenic aerosol effects on snow growth and snowfall rate. *Geophys. Res. Lett.,* **30,** 1538, doi:10.1029/2002GL016855.

Cotton, W. R., G. J. Tripoli, R. M. Rauber, and E. A. Mulvihill, 1986: Numerical simulation of the effects of varying ice crystal nucleation rates and aggregation processes on orographic snowfall. *J. Climate Appl. Meteor.,* **25,** 1658–1680.

Feichter, J., E. Kjellström, H. Rodhe, F. Dentener, J. Lelieveld, and G.-J. Roelofs, 1996: Simulation of the tropospheric sulfur cycle in a global climate model. *Atmos. Environ.,* **30,** 1693–1707.

Greenwald, T. J., G. L. Stephens, T. H. Vonder Haar, and D. L. Jackson, 1993: A physical retrieval of cloud liquid water over the global oceans using Special Sensor Microwave/Imager (SSM/I) observations. *J. Geophys. Res.,* **98,** 18 471–18 488.

Hahn, C. J., S. G. Warren, and J. London, 1994: Climatological data for clouds over the globe from surface observations, 1982–1991: The total cloud edition. Oak Ridge National Laboratory Tech. Rep. ORNL/CDIAC-72 NDP-026A, Oak Ridge, TN, 39 pp.

Hartmann, D. L., 1993: Radiative effects of clouds on earth's climate. *Aerosol–Cloud–Climate Interactions,* P. V. Hobbs, Ed., International Geophysical Series, Vol. 54, Academic Press, 151–173.

Hess, M., P. Koepke, and I. Schult, 1998: Optical properties of aerosols and clouds: The software package OPAC. *Bull. Amer. Meteor. Soc.,* **79,** 831–844.

Houghton, J. T., Y. Ding, D. J. Griggs, M. Noguer, P. J. van der Linden, X. Dai, K. Maskell, and C. A. Johnson, Eds., 2001: *Climate Change 2001: The Scientific Basis.* Cambridge University Press, 881 pp.

Khain, A. P., D. Rosenfeld, and A. Pokrovsky, 2001: Simulating convective clouds with sustained supercooled liquid water down to −37.5°C using a spectral microphysics model. *Geophys. Res. Lett.,* **28,** 3887–3890.

Korolev, A. V., G. A. Isaac, and J. Hallett, 2000: Ice particle habits in stratiform clouds. *Quart. J. Roy. Meteor. Soc.,* **126,** 2873–2902.

——, ——, S. G. Cober, W. Strapp, and J. Hallett, 2003: Microphysical characterization of mixed-phase clouds. *Quart. J. Roy. Meteor. Soc.,* **129,** 39–65.

Kristjánsson, J. E., J. M. Edwards, and D. L. Mitchell, 2000: Impact of a new scheme for optical properties of ice crystals on climates of two GCMs. *J. Geophys. Res.,* **105,** 10 063–10 079.

Lew, J. K., D. C. Montague, and H. R. Pruppacher, 1986: A wind

tunnel investigation on the riming of snowflakes. Part I: Porous disks and large stellars. *J. Atmos. Sci.,* **43,** 2392–2409.
Lin, Y. L., R. D. Farley, and H. D. Orville, 1983: Bulk parameterization of the snow field in a cloud model. *J. Climate Appl. Meteor.,* **22,** 1065–1092.
Liu, Y., and P. H. Daum, 2002: Indirect warming effect from dispersion forcing. *Nature,* **419,** 580–581.
Lohmann, U., 2002a: A glaciation indirect aerosol effect caused by soot aerosols. *Geophys. Res. Lett.,* **29,** 1052, doi:10.1029/2001GL014357.
——, 2002b: Possible aerosol effects on ice clouds via contact nucleation. *J. Atmos. Sci.,* **59,** 647–656.
——, and J. Feichter, 2001: Can the direct and semi-direct aerosol effect compete with the indirect effect on a global scale? *Geophys. Res. Lett.,* **28,** 159–161.
——, and G. Lesins, 2002: Stronger constraints on the anthropogenic indirect aerosol effect. *Science,* **298,** 1012–1016.
——, J. Zhang, and J. Pi, 2003: Sensitivity studies of the effect of increased aerosol concentrations and snow crystal shape on the snowfall rate in the Arctic. *J. Geophys. Res.,* **108,** 4341, doi:10.1029/2003JD003377.
Matveev, L. T., 1984: *Cloud Dynamics.* D. Reidel, 340 pp.
McFarquhar, G. M., P. Yang, A. Macke, and A. J. Baran, 2002: A new parameterization of single scattering solar radiative properties for tropical anvils using observed ice crystal size and shape distributions. *J. Atmos. Sci.,* **59,** 2458–2478.
Mitchell, D. L., 1990: Evolution of snow-size spectra predicted by the growth processes of diffusion, aggregation and riming. Preprints, *Conf. on Cloud Physics,* San Francisco, CA, Amer. Meteor. Soc., 270–277.
Nakajima, T., A. Higurachi, K. Kawamoto, and J. E. Penner, 2001: A possible correlation between satellite-derived cloud and aerosol microphysical parameters. *Geophys. Res. Lett.,* **28,** 1171–1174.
Peng, Y., and U. Lohmann, 2003: Sensitivity study of the spectral dispersion of the cloud droplet size distribution on the indirect aerosol effect. *Geophys. Res. Lett.,* **30,** 1507, doi:10.1029/2003GL017192.
Pruppacher, H. R., and J. D. Klett, 1997: *Microphysics of Clouds and Precipitation.* Kluwer Academic, 954 pp.
Raedel, G., C. J. Stubenrauch, R. Holz, and D. L. Mitchell, 2003: Retrieval of effective ice crystal size in the infrared: Sensitivity study and global measurements from TIROS-N Operational Vertical Sounder. *J. Geophys. Res.,* **108,** 4281, doi:10.1029/2002JD002801.
Ramaswamy, V., and Coauthors, 2001: Radiative forcing of climate change. *Climate Change 2001: The Scientific Basis,* J. T. Houghton et al., Eds., Cambridge University Press, 349–416.
Roeckner, E., and Coauthors, 1996: The atmospheric general circulation model ECHAM4: Model description and simulation of the present day climate. Max Planck Institute for Meteorology Tech. Rep. 218, Hamburg, Germany, 90 pp.
Rogers, R. R., and M. K. Yau, 1989: A *Short Course in Cloud Physics.* 3d ed. Pergamon, 293 pp.
Rossow, W. B., and R. A. Schiffer, 1999: Advances in understanding clouds from ISCCP. *Bull. Amer. Meteor. Soc.,* **80,** 2261–2287.
Stendel, M., and K. Arpe, 1997: Evaluation of the hydrological cycle in reanalysis and observations. Max Planck Institute for Meteorology Tech. Rep. 228, Hamburg, Germany, 52 pp.
Sundqvist, H., E. Berge, and J. E. Kristiansson, 1989: Condensation and cloud parameterization studies with a mesoscale numerical weather prediction model. *Mon. Wea. Rev.,* **117,** 1641–1657.
Weng, F., and N. C. Grody, 1994: Retrieval of cloud liquid water using the special sensor microwave imager (SSM/I). *J. Geophys. Res.,* **99,** 25 535–25 551.
Wentz, F. J., 1997: A well-calibrated ocean algorithm for SSM/I. *J. Geophys. Res.,* **102,** 8703–8718.